ACS APPLIED MATERIALS & INTERFACES

Research Article

www.acsami.org

High Catalytic Activity of Amorphous Ir-Pi for Oxygen Evolution Reaction

Ahamed Irshad and Nookala Munichandraiah*

Department of Inorganic and Physical Chemistry, Indian Institute of Science, Bangalore-560012, India

Supporting Information

ABSTRACT: Large-scale production of hydrogen gas by water electrolysis is hindered by the sluggish kinetics of oxygen evolution reaction (OER) at the anode. The development of a highly active and stable catalyst for OER is a challenging task. Electrochemically prepared amorphous metal-based catalysts have gained wide attention after the recent discovery of a cobalt-phosphate (Co-Pi) catalyst. Herein, an amorphous iridium-phosphate (Ir-Pi) is investigated as an oxygen evolution catalyst. The catalyst is prepared by the anodic polarization of carbon paper electrodes in neutral phosphate buffer solutions containing $IrCl_3$. The Ir-Pi film deposited on the substrate has significant amounts of phosphate and Ir centers in an oxidation state higher than +4. Phosphate plays a significant role in the deposition of the catalyst and also in its activity toward OER. The onset potential of OER on the Ir-Pi is about 150 mV lower in comparison with the Co-Pi under identical experimental conditions. Thus, Ir-Pi is a promising catalyst for electrochemical oxidation of water.

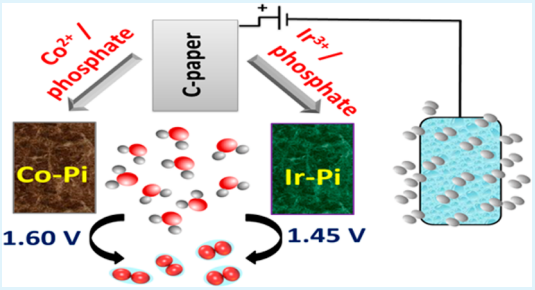

KEYWORDS: *Ir-Pi catalyst, electrochemical deposition, water oxidation, electrolysis of water, phosphate buffer, hydrogen generation, amorphous catalysts*

1. INTRODUCTION

A high energy density and eco-friendliness make hydrogen as an attractive fuel to meet the increased energy demands of the future.[1,2] Although, hydrogen is produced on large scale by steam-methane reforming route at present,[3,4] huge amount of carbon dioxide is released into the atmosphere as a byproduct, thus resulting in environmental concerns. Development of alternate clean methods to produce H_2 is a challenge for the successful realization of hydrogen economy.

Production of hydrogen gas by electrolysis of water is a well-known process. The process involves oxygen evolution reaction (OER) at the anode and hydrogen evolution reaction (HER) at the cathode. The Gibbs free energy change (ΔG) of the overall reaction is 237 kJ mol^{-1}.[5] Accordingly, a thermodynamic voltage of 1.23 V is calculated from the relationship, $\Delta G = -nFE$, as the minimum voltage required for electrolytic decomposition of H_2O into H_2 and O_2. However, commercial electrolyzers usually operate between 1.8 to 2.1 V,[6,7] indicating the necessity of large overvoltages to drive the reactions at a sufficiently fast rates. The high overvoltage and subsequent energy loss are mainly associated with the sluggish kinetics of water oxidation reaction at the anode.[8,9] The overvoltage can be considerably reduced using suitable catalysts. Hence, the design of stable, robust, and efficient OER catalysts is an important task to improve the performance of electrolyzers, which leads to a cost-effective production of hydrogen.

Various materials, mainly metal oxides,[10] have been studied widely as OER catalysts. Among theses, oxides of Ru and Ir are the most active.[11,12] However, RuO_2 undergoes corrosion at high anodic potentials due to the formation of RuO_4.[13] However, IrO_2 is stable[14] and exhibits metallic conductivity.[15] IrO_2 is generally prepared by various methods such as metal organic chemical vapor deposition,[16,17] thermal oxidation[18,19] and electrodeposition.[20,21] Among these methods, electrodeposition has many advantages such as control on the morphology, crystalinity, chemical composition and specific mass. Moreover, it is reported that amorphous oxides prepared at low temperatures are more active than the crystalline oxides prepared at high temperatures.[22,23] This is due to high density of surface defects and coordinatively unsaturated sites in amorphous phase. Such sites are chemically very active and facilitate the adsorption of reactant molecules and intermediates, resulting in overall enhancement in the reaction rate.[24] In a study on RuO_2, it was proposed that local structural flexibility in amorphous material is the decisive factor for their superior activity because local structure of the adsorption site may be easily distorted by the formation of intermediates, causing drastic change in the performance.[25] In another study on $CoWO_4$, the superior activity of amorphous phase over crystalline phase was attrtibuted to differences in the reaction mechanism.[26] In addition to high activity, amorphous oxides can also be formed with wide composition ranges unlike in crystalline forms, thus making it easier to tune their electronic properties. Therefore, it is desirable to prepare highly active

Received: March 25, 2015
Accepted: July 1, 2015
Published: July 1, 2015

DOI: 10.1021/acsami.5b02601
ACS Appl. Mater. Interfaces 2015, 7, 15765−15776

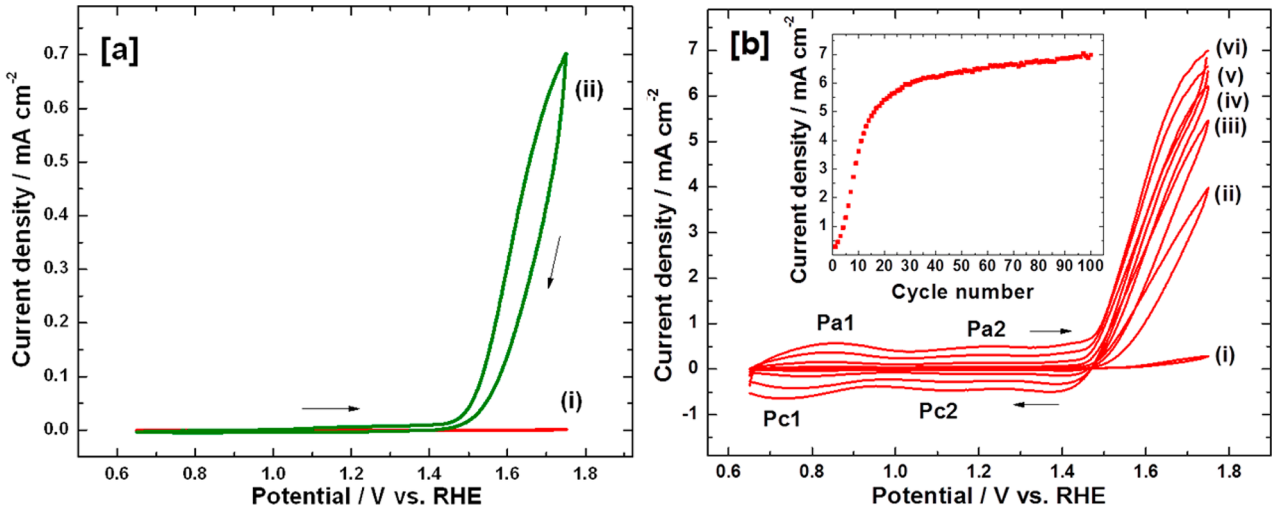

Figure 1. (a) Cyclic voltammograms of carbon paper electrodes in 0.1 M neutral phosphate buffer solutions (i) without $IrCl_3$ and (ii) with 0.5 mM $IrCl_3$. (b) Cyclic voltammograms of carbon paper electrode in 0.5 mM $IrCl_3$ + 0.1 M phosphate buffer solution (pH 7.0) after (i) 1, (ii) 10, (iii) 20, (iv) 40, (v) 70, and (vi) 100 cycles. Inset shows the plot of current density at 1.75 V against cycle number. Scan rate: 5 mVs^{-1}.

amorphous Ir-based OER catalysts by electrodeposition method.

In recent years, electrodeposition of amorphous metal-based catalysts from buffer solutions has gained widespread interest,[27,28] especially after the discovery of a cobalt phosphate catalyst (Co-Pi) in 2008 by Kanan and Nocera.[29] Following this report, numerous other similar catalysts have been studied. It is observed that anodic polarization of substrate electrodes in solutions consisting of metal ions such as Co^{2+},[29,30] Mn^{2+},[31,32] Fe^{2+},[33] Ni^{2+},[34,35] and Cu^{2+}[36] in buffer media such as acetate, phosphate, borate, etc., leads to the deposition of active catalysts composed of the corresponding anions (phosphate, acetate or borate). These materials are reported to have clusters of interconnected complete or incomplete metal-oxo/hydroxo cubanes with terminal ligation to the electrolyte species.[37,38] Such catalysts are promising owing to their high activity and self-repairing property.[39,40] However, studies reported until now are restricted to a few first row transition metals and attempts have not been made using second or third row transition elements, such as Ru, Ir, etc. Since, the intrinsic activity of Ir is superior to Co, it is expected that a highly active catalyst can be designed by replacing Co in the Co-Pi with Ir. Furthermore, such a catalyst will be useful for the comparison and structure−activity correlation among similar catalysts that differ only at their metal centers.

To the best of author's knowledge, there are no systematic studies reported on the electrochemical deposition of Ir-based OER catalysts from phosphate buffer solutions. In the present study, the electrochemical deposition of a highly active catalyst (Ir-Pi) from a neutral phosphate buffer solution containing Ir^{3+} is undertaken. The catalytic activity of Ir-Pi is far superior to Co-Pi toward OER.

2. EXPERIMENTAL SECTION

Analytical grade KH_2PO_4, K_2HPO_4, KNO_3 (all from Merck), and $IrCl_3$ (Aldrich) were used as received. All solutions were prepared in doubly distilled water. Phosphate buffer solution was prepared by mixing 0.1 M KH_2PO_4 and 0.1 M K_2HPO_4 solution. The pH of buffer solution was maintained at 7.0, unless otherwise stated. A Toray carbon paper of thickness 0.2 mm was used as the substrate for the preparation of electrodes. A strip of 7 mm width and 3 cm length was cut from a carbon paper sheet and 1.4 cm^2 area at one of the ends was exposed to the electrolyte. The rest of its length was used for electrical contact. The unused area of the electrode was masked by PTFE tape. Pt foil auxiliary electrodes and saturated calomel reference electrode (SCE) were used in a glass cell. Microscopic analysis was carried out by using Ultra 55 scanning electron microscope (SEM) equipped with energy dispersive X-ray analysis (EDXA) system at 20 kV. Powder X-ray diffraction (XRD) patterns were recorded by Bruker D8 diffractometer using Cu K_α radiation The surface compositions of the materials were analyzed by X-ray photoelectron spectroscopy (XPS) using SPECS GmbH spectrometer (Phoibos 100 MCD Energy Analyzer) with Mg K_α radiation (1253.6 eV). The peak of C 1s at 284.6 eV was considered as the reference position. Electrochemical experiments were carried out using PARC EG&G potentiostat/galvanostat model Versastat II. Mass variations during electrochemical depositions were monitored using CH Instruments potentiostat/galvanostat model 440A equipped with electrochemical quartz crystal microscope (EQCM). A small Teflon cell with Au-coated quartz crystal (8 M Hz, active area = 0.205 cm^2, sensitivity = 0.146 Hz ng^{-1} cm^2) as the working electrode, a Pt wire counter electrode and Ag/AgCl, Cl^- (3M) reference electrode was used. Oxygen produced during electrolysis was probed by monitoring its reduction at a platinum disc electrode of area 0.07 cm^2 (diameter- 3 mm) in an airtight glass cell. Electrochemical impedance spectroscopy (EIS) measurements were conducted at an ac excitation signal of 10 mV over the frequency range from 100 kHz to 0.10 Hz. All electrochemical experiments were performed at 22 ± 1 °C. Current density values are reported on the basis of geometrical area of the electrode. All potential values are reported against RHE reference.

3. RESULTS AND DISCUSSION

3.1. Electrochemical Deposition of Ir-Pi Catalyst. Cyclic voltammograms of carbon paper electrodes in 0.1 M phosphate buffer (pH 7.0) solutions in the absence and presence of 0.5 mM $IrCl_3$ are shown in Figure 1a. In the absence of Ir^{3+} (Figure 1a(i)), negligibly small current flows, indicating the absence of any electrochemical reaction in the potential range 0.65−1.65 V. On the other hand, the voltammogram in the presence of Ir^{3+} (Figure 1a(ii)) exhibits a sharp increase in the current at 1.45 V which accompanies an evolution of oxygen (visual observation) at the electrode surface. It is thus understood that an Ir-based OER catalyst (Ir-Pi) starts forming at 1.45 V and concomitantly it catalyzes the OER (reaction 1).

DOI: 10.1021/acsami.5b02601
ACS Appl. Mater. Interfaces 2015, 7, 15765−15776

$$4OH^- \rightarrow 2H_2O + O_2 + 4e^- \quad (1)$$

Formation and catalytic activity of Ir-Pi are similar to those of Co-Pi catalyst,[29] but the potential of the later is about 1.60 V instead of 1.45 V for the Ir-Pi catalyst (Figure 1a(ii)). Thus, the catalytic activity of Ir-Pi is greater than that of Co-Pi catalyst. A carbon paper electrode was repeatedly cycled in 0.1 M phosphate buffer solution containing 0.5 mM $IrCl_3$. Typical voltammograms are shown in Figure 1b. There is an increase in voltammetric current in the potential region of OER on potential cycling. A plot of current density at 1.75 V versus number of cycles is presented in Figure 1b inset. There is a sharp increase in current over the first 20 cycles and a gradual increase thereafter. The increase in current is attributed to increased coverage on the current collector as well as the thickness of the Ir-Pi catalyst layer, which in turn enhance the rate of OER. Increased evolution of O_2 gas was visually observed in the potential range 1.45−1.75 V on repeated cycling. Although no current peaks corresponding to Ir^{3+} oxidation are observed in the initial stages of cycling (Figure 1a(ii)), two pairs of peaks appear after repeated cycling (Figure 1b). The broad and reversible peaks (Pa1 and Pc1) at about 0.85 V is attributed to the Ir^{3+}/ Ir^{4+} redox couple and the other pair (Pa2 and Pc2) at 1.23 V is to Ir^{4+}/ Ir^{5+} redox couple.[41] Both the pairs of peaks are very broad indicating the formation various hydrated structures that differ slightly in their redox behavior.[42] Thus, the Ir-Pi catalyst can be considered to be a highly hydrated oxide with Ir centers in an oxidation state higher than +4.

It was intended to study the role of phosphate ions in the electrodeposition and OER catalysis. Cyclic voltammetry experiments were carried out in 0.1 M KNO_3 solutions (pH 7.0) and the results are shown in Figure 2. In the absence of

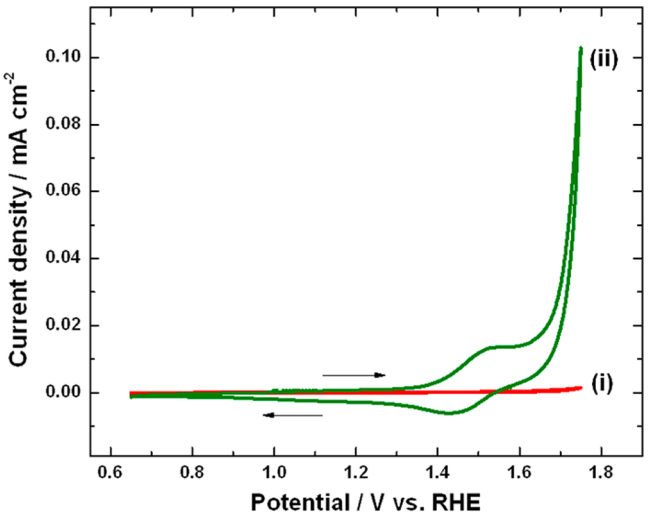

Figure 2. Cyclic voltammograms of carbon paper electrodes in 0.1 M KNO_3 solutions (i) without $IrCl_3$ and (ii) with 0.5 mM $IrCl_3$. Scan rate: 5 mV s^{-1}.

Ir^{3+}, the magnitude of current is negligibly small in the potential range 0.65−1.75 V (Figure 2(i)). However, in the presence of 0.5 mM $IrCl_3$ (Figure 2(ii)), a diffusion controlled current peak appears at 1.53 V corresponding to the oxidation of Ir^{3+} and subsequent deposition of IrO_2 on the electrode surface. This is followed by an increase in the current due to the oxidation of water. The onset potential for OER is 1.60 V, which is 150 mV higher than the onset potential in phosphate buffer solution (Figure 1a(ii)). Furthermore, the catalytic current observed at 1.75 V is only 0.1 mA cm^{-2} (Figure 2(ii)), which is significantly less than 0.7 mA cm^{-2} (Figure 1a(ii)) obtained in the phosphate medium under identical conditions. Thus, the catalyst Ir-Pi prepared from phosphate buffer solution is superior to the catalyst IrO_2 prepared from KNO_3 solution.

Electrolysis experiments were performed both in phosphate and nitrate solutions consisting of 0.5 mM $IrCl_3$ at 1.65 V for 12 h. During the deposition from phosphate solution containing 0.5 mM $IrCl_3$ (Figure 3(i)), there is a steep increase

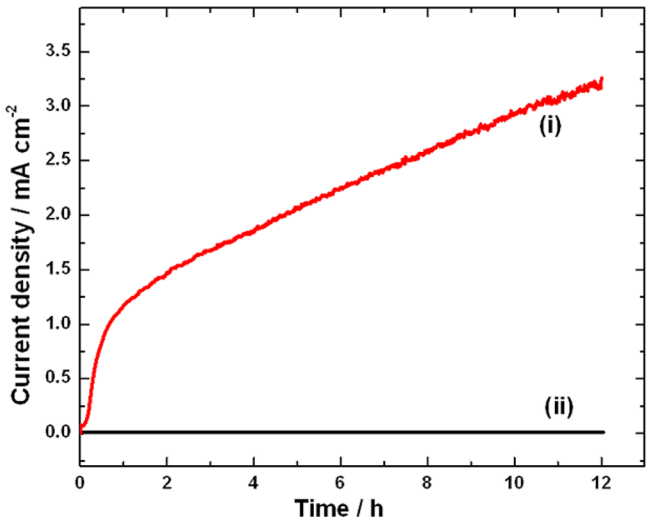

Figure 3. Current versus time plot during electrolysis at 1.65 V in (i) 0.5 mM $IrCl_3$ + 0.1 M phosphate and (ii) 0.5 mM $IrCl_3$ + 0.1 M KNO_3. pH was adjusted to 7.0 in both the cases.

in the current density to 1.2 mA cm^{-2} within the first 1 h and thereafter, current rises gradually to 3.2 mA cm^{-2} at 12 h. During this process, a steady growth of Ir-Pi catalyst was visually observed along with an increased evolution of oxygen gas. Catalytic activity of the Ir-Pi was evident from this experiment as there were no gas bubbles seen on the electrode surface in the initial stage and oxygen evolution became increasingly vigorous with time. During a similar experiment in 0.1 M KNO_3 solution containing 0.5 mM $IrCl_3$ (Figure 3(ii)), a negligibly small current was observed throughout the electrolysis. Current density reaches only 13 μA cm^{-2} after 12 h, which is 250 times smaller than the current observed in the phosphate solution under identical experimental conditions. These results suggest that the electrodeposition from phosphate buffer solution is advantageous and the catalytic activity of Ir-Pi is greater than IrO_2 toward OER.

It was intended to investigate the effect of concentration of Ir^{3+} ions on the electrochemical deposition of Ir-Pi and OER activity. For this purpose, amperometry experiments were carried at 1.55 V for 30 min in 0.1 M phosphate buffer solution (pH 7.0) containing various concentrations of $IrCl_3$ ranging from 0.5 to 5 mM. Such studies are considered as important as the solubility of most of the metal ions such as Co^{2+}, Mn^{2+}, Ni^{2+}, etc. are limited to about 0.5 mM in neutral phosphate solutions. Higher solubility is advantageous as the rate of electrochemical deposition becomes fast by increasing the concentration. It is seen from Figure 4a that the current density value after 30 min of Ir-Pi deposition is only 0.42 mA cm^{-2} in 0.5 mM $IrCl_3$ solution whereas it is 0.63, 0.79, 1.07, 1.47, and

DOI: 10.1021/acsami.5b02601
ACS Appl. Mater. Interfaces 2015, 7, 15765−15776

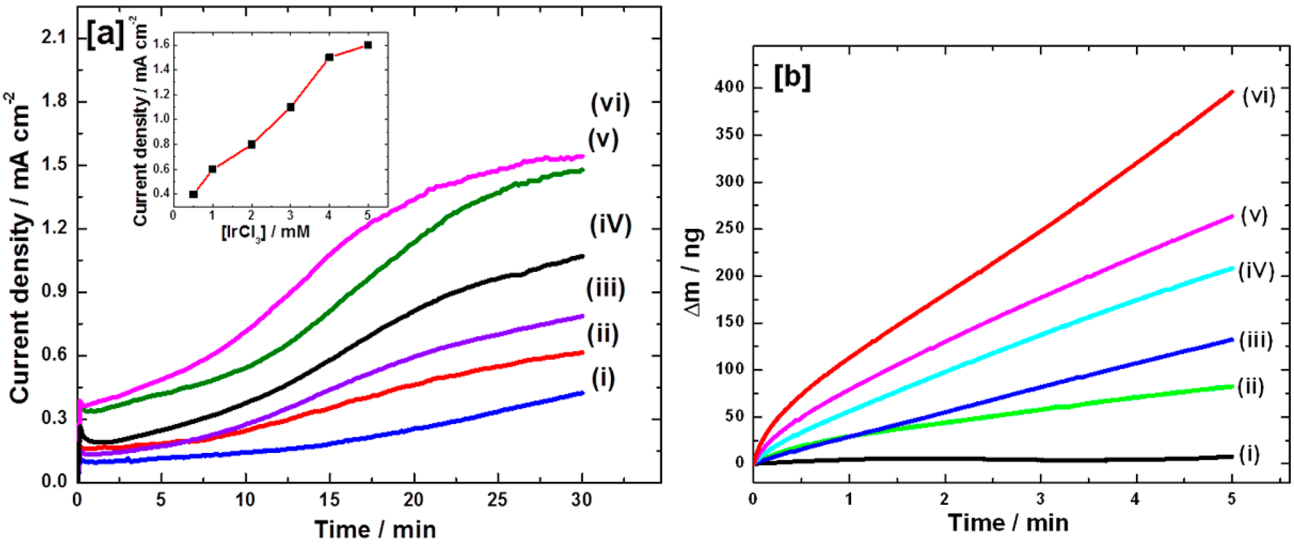

Figure 4. (a) Current versus time plots during the deposition of Ir-Pi catalyst on carbon paper electrode at 1.55 V for 30 min from 0.1 M phosphate solutions (pH 7.0) containing (i) 0.5, (ii) 1, (iii) 2, (iv) 3, (v) 4, and (vi) 5 mM $IrCl_3$. Inset shows the variation in the current density after 30 min of deposition as a function of $IrCl_3$ concentrations (b) Mass variation versus time plots during Ir-Pi deposition on a gold coated quartz crystal electrode of area 0.205 cm^2 at 1. 50 V for 5 min in 0.1 M neutral phosphate solutions containing (i) 0, (ii) 0.1, (iii) 0.2, (iv) 0.5, (v) 2, and (vi) 5 mM $IrCl_3$.

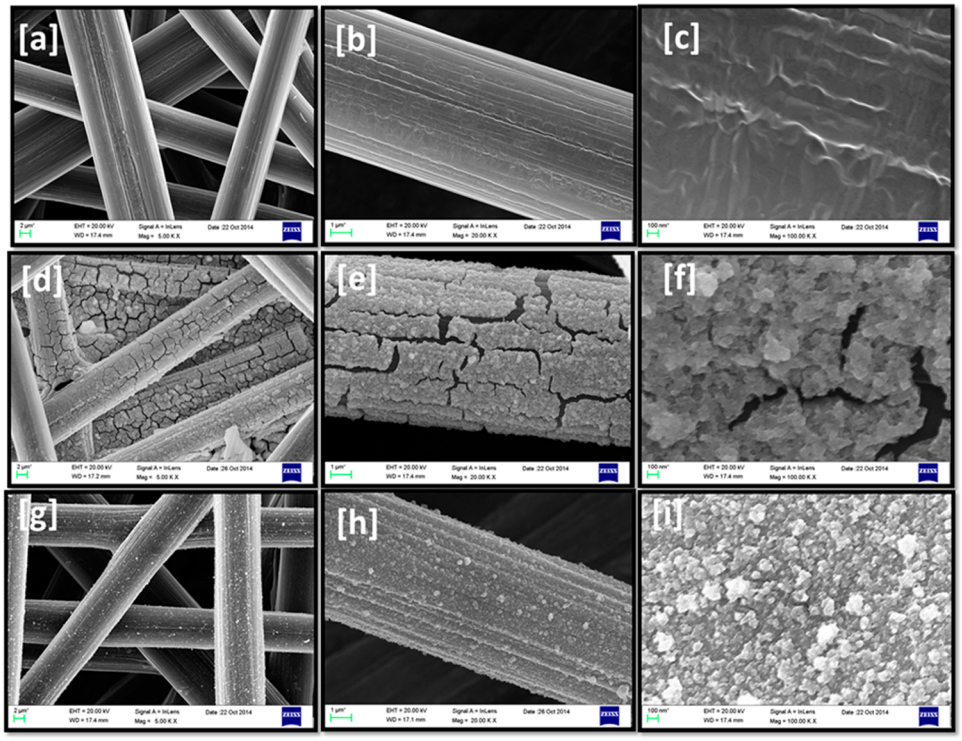

Figure 5. SEM images of (a–c) bare carbon paper, (d–f) Ir-Pi/C, and (g–i) IrO_2/C.

1.55 mA cm^{-2}, respectively, in 1, 2, 3, 4, and 5 mM $IrCl_3$ solutions. Thus, the current increases almost linearly (Figure 4a inset) with concentration. Mass variations of Au-coated quartz crystal electrodes were also recorded in situ during the deposition of Ir-Pi for different concentrations of $IrCl_3$ using EQCM (Figure 4b). The results show that the mass of the catalyst after 5 min of electrolysis at 1.50 V is only 80 ng when the concentration of $IrCl_3$ is 0.1 mM (Figure 4b(ii)) and it is almost 5 times greater at 5 mM (Figure 4b(vi)). Similar experiments at 0.2, 0.5, and 2 mM $IrCl_3$ solutions resulted in net mass gain of 134, 207, and 265 ng, respectively, (Figure 4b (iii–v)). These results support that the rate of electrodeposition of Ir-Pi can be significantly enhanced by increasing the Ir^{3+} concentration.

3.2. Physical Characterization. The morphology of Ir-Pi catalyst was studied by using SEM. The Toray carbon paper substrate has numerous carbon fibers oriented in different directions (Figure 5a–c). Higher magnification image (Figure 5c) shows kinks and defects that facilitate the adherence of electrodeposits. To study the morphology of Ir-Pi catalyst, SEM micrographs were recorded after 12 h of electrodeposition at 1.65 V in 0.1 M phosphate buffer solution containing 0.5 mM

DOI: 10.1021/acsami.5b02601
ACS Appl. Mater. Interfaces 2015, 7, 15765–15776

$IrCl_3$. Carbon fibers are covered with Ir-Pi flakes (Figure 5d and e) with numerous agglomerated particles. Cracks are observed at higher magnifications (Figure 5e and f). These cracks are formed due to the loss of water on drying the electrodeposits. Furthermore, SEM micrographs were also recorded after 12 h of electrodeposition at 1.65 V from 0.1 M KNO_3 solution containing 0.5 mM $IrCl_3$ (Figure 5g–i). Carbon fibers are decorated with an electrodeposit. However, unlike in the case of Ir-Pi, IrO_2 prepared from KNO_3 solution does not form as islands separated by cracks. Instead, there are tiny particles aggregated together forming clusters. These studies suggest that electrodeposited layers from phosphate and nitrate solutions differ in their morphology.

Powder XRD patterns were recorded for the carbon paper substrate before and after deposition of Ir-Pi catalyst. It is seen from Figure 6i that the pattern for the bare substrate consists of

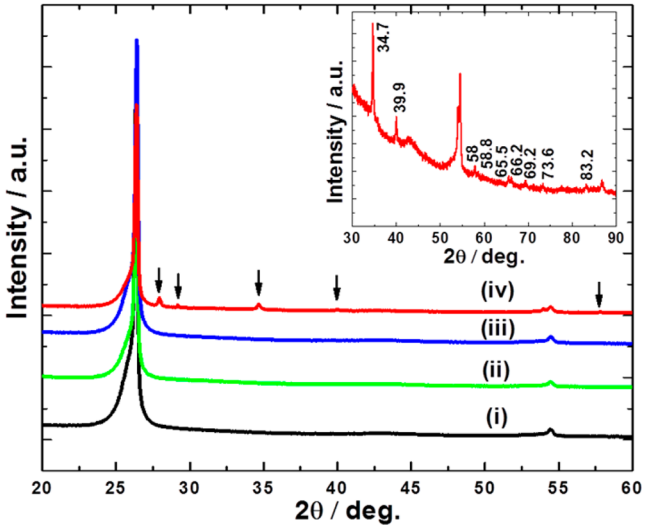

Figure 6. XRD pattern for (i) bare C, (ii) Ir-Pi/C, (iii) IrO_2/C, and (iv) Ir-Pi/C heated at 500 °C for 5 h in air. Inset is expanded view of pattern (iv) in 2θ range 30–90°.

peaks at 2θ = 26.3° and 54.4° due to carbon crystallites. Only these peaks are observed after electrodeposition of Ir-Pi (Figure 6ii) and IrO_2 (Figure 6iii). These results indicate the amorphous nature of the materials deposited from both phosphate and nitrate solutions. Since both Ir-Pi and IrO_2 are amorphous, higher OER activity of Ir-Pi over IrO_2 cannot be attributed to any difference in their crystalinity. However, when the Ir-Pi or IrO_2 was heated at 500 °C for 5 h in air, additional peaks appear due to the formation of crystalline IrO_2 (Figure 6iv and inset). Nevertheless, it is found that the OER catalytic activity of Ir-Pi is considerably reduced after crystallization (Supporting Information (SI), Figure S1).

The compositions of the electrodeposited materials were analyzed by EDXA and XPS techniques. The EDXA spectra were recorded from different regions of the samples. Results are shown in Figure 7. In the case of electrodeposited Ir-Pi catalyst, Ir, P, O and K are identified as major elements (Figure 7a–d). The ratio of Ir:P varies from 1:1.5 to 1:2, indicating a significant amount of phosphate ion incorporated in the catalyst. The elemental maps shown in Figure 7c and d for Ir and P, respectively, indicate a uniform distribution of the elements. Similarly, the IrO_2 electrodeposited from KNO_3 solution shows the presence of Ir, O, and K in the EDXA spectrum (Figure 7e). Trace amount of Cl is also present. The elements are uniformly distributed as evident from X-ray maps (Figure 7g and h). Thus, the significant difference between Ir-Pi and IrO_2 is that the former has a large quantity of phosphate.

Figure 8 shows the XPS spectra of Ir-Pi catalyst which was deposited on carbon paper substrate at 1.70 V for 3 h from a neutral phosphate buffer solution containing 0.5 mM $IrCl_3$. The survey spectrum (Figure 8a) identifies Ir, P, O, C, and K as the major constituents, which are in good agreement with EDXA results. Additionally, photoelectron peaks corresponding to Cl was also noticed. This could be due to surface adsorption of Cl^- from $IrCl_3$ in the electrolyte. In the Ir 4f region (Figure 8b), strong doublet peaks are present at 62.4 and 65.4 eV, which correspond to Ir $4f_{7/2}$ and $4f_{5/2}$, respectively.[43] The Ir 4f core level exhibits a typical line shape with $4f_{5/2}$ peak more intense than the $4f_{7/2}$ signal and the splitting of the spin–orbit doublet at 3.0 eV (Figure 8b). The peak tailing at high energy side of the Ir 4f is attributed to loss of kinetic energy of photoelectrons by interaction with valence band levels.[44] The high resolution P 2p peak (Figure 8c) at 133.1 eV is assigned to phosphate.[45] This is slightly at higher binding energy (0.3 eV) than the P 2p peak observed in the case of Co-Pi deposited on carbon paper.[30] Hence, a weak interaction between the phosphate groups and metal centers in the catalyst is expected. The O 1s peak is located at 531.7 eV (Figure 8d), which is usually observed in the case of Ir–OH.[46] Similarly, K 2p spectrum (Figure 8e) shows doublets with spin orbit splitting of 3.0 eV. The peaks at 292.6 and 295.6 eV are assigned to K $2p_{1/2}$ and $2p_{3/2}$, respectively.[47] Although, the exact chemical identity of K is not evident from XPS, it is likely that K exist in ionic form to maintain the charge balance.

3.3. Catalytic Activity. The electrochemical activity of the Ir-Pi catalyst toward OER in phosphate electrolyte in the absence $IrCl_3$ was investigated. Phosphate buffer solution was chosen for comparison of the present results with the data of well-studied catalyst, namely, Co-Pi. Absence of Ir^{3+} ion in the electrolyte prevents the deposition of the catalyst during OER studies and thus, the resultant current will be a direct measure of the catalytic activity. Ir-Pi was deposited at 1.55 V for 1000 s from phosphate buffer solution containing 0.5 mM $IrCl_3$. For comparison, IrO_2 was also deposited under identical condition except that the supporting electrolyte was KNO_3 solution instead of phosphate buffer solution. Electrodes were thoroughly rinsed with double distilled water and dried in air. Then, the electrodes were subjected to linear sweep voltammetry at 5 mV s^{-1} in phosphate buffer solution (Figure 8). There is no current flow at Ir-Pi coated electrode until the potential reaches 1.45 V, when the current raises rapidly and reaches 2.2 mA cm^{-2} at 1.65 V due to OER (Figure 9i). The onset potential of OER is as low as 1.45 V indicating an overpotential of 220 mV. Vigorous evolution of O_2 on the electrode was observed at the potential region between 1.50 and 1.65 V. On the other hand, IrO_2 electrode shows much less activity (Figure 9ii). No oxygen evolution was visually observed until potential reached 1.65 V. The current density at 1.65 V is only 0.5 mA cm^{-2}, which is about 4.5 times lower than that of Ir-Pi. Although the electrochemical acive surface area of the Ir-Pi deposit is found to be about 2.8 times higher in comparison with that of IrO_2 (SI, Figure S2), it alone cannot explain 4.5 times higher activity of Ir-Pi over IrO_2. Hence, the superior OER activity of the Ir-Pi is due to both high active surface area and high intrinsic catalytic effect. The OER activity of Ir-Pi was further compared with that of Co-Pi catalyst, which has been

DOI: 10.1021/acsami.5b02601
ACS Appl. Mater. Interfaces 2015, 7, 15765–15776

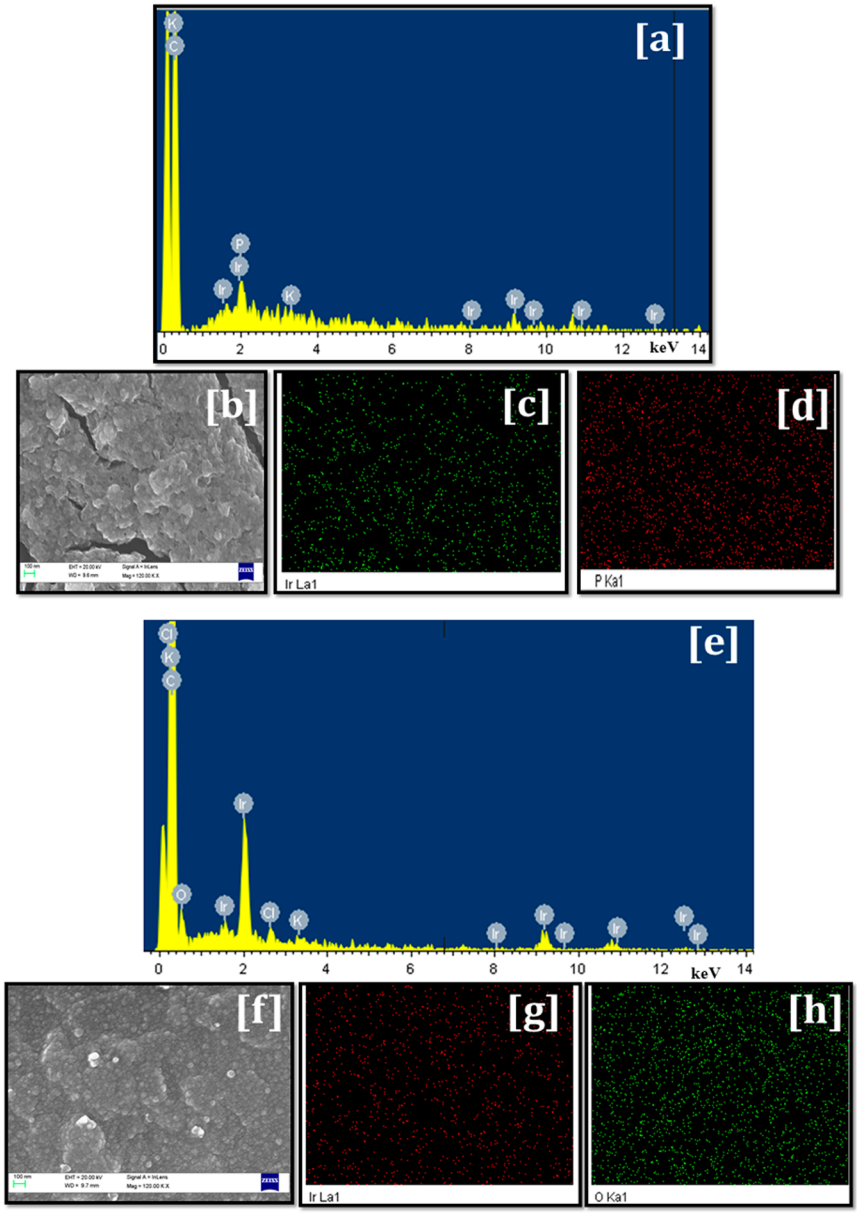

Figure 7. EDXA spectra for (a) Ir-Pi/C and (e) IrO_2/C. (b) SEM image of the Ir-Pi catalyst and elemental map showing the distribution of (c) Ir and (d) P. (f) SEM image of the IrO_2 catalyst and elemental map showing the distribution of (g) Ir and (h) O.

considered as the benchmark catalyst for OER in neutral medium.[29] For this, Co-Pi was deposited under similar condition as that of Ir-Pi and then, the electrode was subjected to LSV in phosphate electrolyte (Figure 9iii). It is seen from Figure 9iii that the onset of OER on Co-Pi occurs at 1.57 V. This value is 120 mV higher than that for Ir-Pi. Moreover, current is only 0.3 mA cm^{-2} at 1.65 V, which is significantly smaller than the current (2.2 mA cm^{-2}) obtained on Ir-Pi electrode. Thus, Ir-Pi is superior to Co-Pi both in terms of OER onset potential and current density at any potential in the OER region. Ir-Pi deposited on FTO coated glass also shows the similar catalytic properties (SI, Figure S3).

The O_2 evolved by water oxidation on Ir-Pi catalyst was probed by its reduction on a Pt rotating disc electrode (RDE) in an airtight glass cell. An Ir-Pi coated carbon paper electrode was prepared at 1.60 V for 1 h from 0.5 mM $IrCl_3$ + 0.1 M phosphate buffer solution (pH 7.0). An electrochemical cell was assembled in phosphate buffer solution with both Ir-Pi coated carbon paper and a Pt RDE as working electrodes. The electrolyte was purged with Ar and the potential of Pt RDE was swept at 10 mV s^{-1} from 1.05 to 0.15 V at 2500 rpm. Negligibly small current flows (Figure 10a(i)), indicating the removal of dissolved O_2 from the electrolyte by purging with Ar. Then, electrolysis was conducted at the Ir-Pi coated carbon paper electrode at 1.75 V. After 1 h, the electrolysis was terminated and the Pt RDE was again subjected to linear sweep voltammetry. It was seen (Figure 10a(ii)) that the current due to ORR increased to 0.2 mA cm^{-2} at 0.15 V. This indicated that the O_2 evolved on Ir-Pi electrode during electrolysis and the dissolved O_2 underwent reduction subsequently at the RDE. Electrolysis was again continued at the Ir-Pi and the voltammogram of ORR was recorded after every 1 h of electrolysis. As observed in Figure 10a(iii) and (iv), the ORR current increased to 0.3 and 0.4 mA cm^{-2}, respectively, after 2 and 3 h of OER. Finally, the electrolyte was saturated with pure O_2 gas from a cylinder and again the Pt RDE was subjected to

DOI: 10.1021/acsami.5b02601
ACS Appl. Mater. Interfaces 2015, 7, 15765−15776

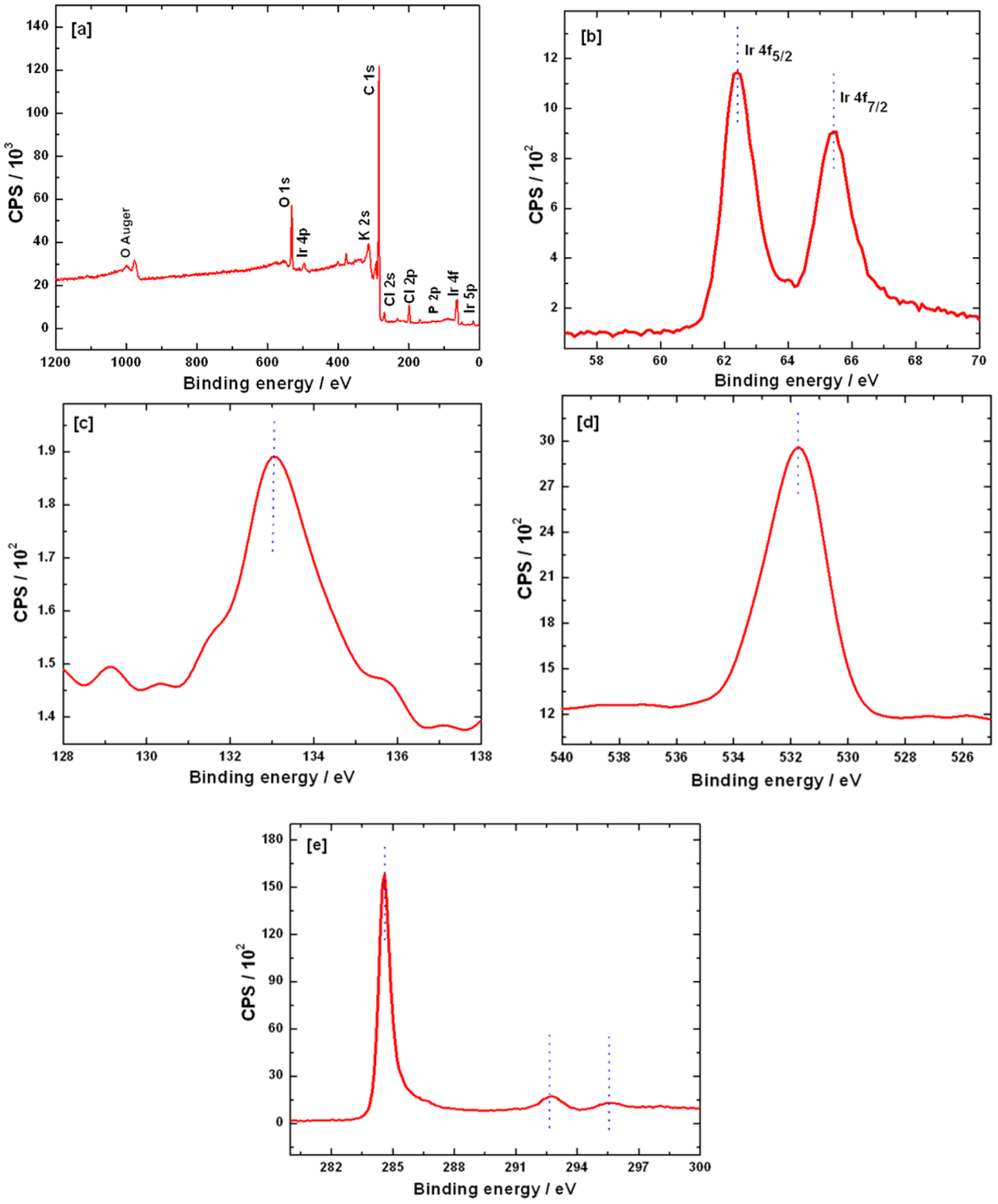

Figure 8. XPS spectra of Ir-Pi catalyst. (a) Survey spectrum and high resolution spectra for (b) Ir 4f, (c) P 2p, (d) O 1s, and (e) K 2p.

linear sweep voltammetry. The reduction current increased in magnitude (Figure 10a(v)). These studies confirm that the electrolysis product at Ir-Pi was oxygen. It is worth noticing that ORR current on the Pt electrode measured at 0.15 V varies linearly with the time of electrolysis on Ir-Pi (Figure 10b(i)), indicating a constant rate of oxygen evolution and a high stability of the Ir-Pi catalyst during water electrolysis condition. Similar experiments were repeated with bare carbon electrode instead of Ir-Pi coated carbon paper electrode. Current was negligibly small (Figure 10b(ii)) during the entire period of experiment, indicating a poor catalytic activity of the carbon paper substrate toward OER.

To study the effect of thickness of the catalyst toward OER, Ir-Pi was deposited in various thicknesses on carbon paper electrodes from 0.5 mM $IrCl_3$ in 0.1 M phosphate solution by passing charges in the range from 50 to 1000 mC cm^{-2}. The electrodes were washed well with double-distilled water and dried. The catalytic activity was studied by linear sweep

DOI: 10.1021/acsami.5b02601
ACS Appl. Mater. Interfaces 2015, 7, 15765−15776

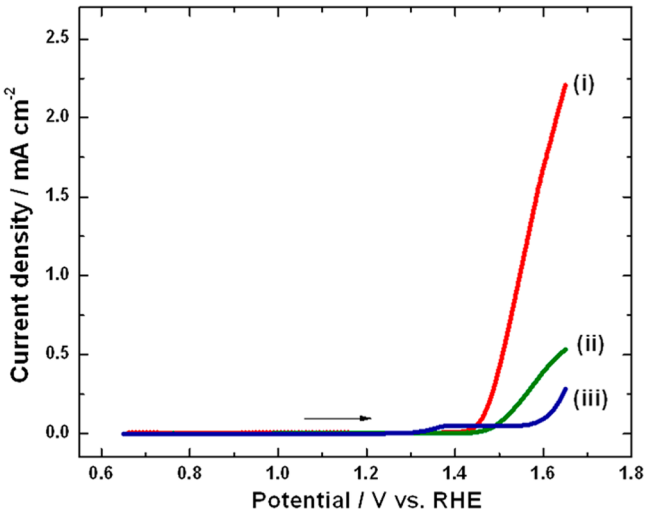

Figure 9. Linear sweep voltammograms of carbon paper electrodes coated with (i) Ir-Pi, (ii) IrO_2, and (iii) Co-Pi in 0.1 M phosphate electrolyte (pH 7.0). Catalysts were deposited at 1.55 V for 1000 s from the corresponding electrolytes with 0.5 mM metal salts.

voltammetry at 0.05 mV s^{-1} in phosphate buffer electrolyte under stirring (Figure 11a). It is observed that the catalytic activity increases with an increase in the catalyst loading. This is attributed to an increase in coverage of the catalyst on the substrate and also in the density of surface active sites with an increase in thickness. The values of current density measured at 1.55 V are 0.04, 0.11, 0.33, 0.47, and 0.94 mA cm^{-2}, respectively, for the Ir-Pi prepared by passing 50, 100, 200, 500, and 1000 mC cm^{-2} (Figure 11a, curves ii–vi). Negligibly small current flows for bare carbon signifying the inertness of the carbon paper substrate toward OER (Figure 11a, curve i. The Tafel plots are shown in Figure 11b. The Tafel slope are 59, 56, 55, 56, and 67 mV $decade^{-1}$, respectively, for Ir-Pi catalysts prepared using charge 50, 100, 200, 500, and 1000 mC cm^{-2}. Thus, the Tafel slope is independent of thickness and the average slope is closer to 2.3 × RT/F. This suggests that OER mechanism involves a reversible one-electron and one proton transfer process prior to the rate limiting step.[48]

The pH dependence of Ir-Pi catalyst was examined by constant potential electrolysis in 0.1 M phosphate solution. The potential was fixed at 1.50 V while the solution pH was gradually increased from 5 to 13. Then, the steady state current was measured at each pH value. A plot of the log (current density) vs pH (Figure 11c) exhibits a straight line in the range of pH 5.0 to 8.0 with a slope of 1.0, whereas a deviation from linearity is observed beyond this range. This could be due to the poor buffer capacity of the solution. In addition, the pH dependence was also studied using galvanostatic titration method. A constant current of 100 μA cm^{-2} was passed and the corresponding potential was measured while the pH was gradually increased from 4.5 to 13 (Figure 11d). A linear fit of the data in Figure 11d yields a slope of 59 mV. Tafel slope (Figure 11b is related to the slopes of potential versus pH (Figure 11d) and log (current density) versus pH (Figure 11c) plots using the following equation:[48]

$$(\partial E/\partial \mathrm{pH})_i = (\partial E/\partial \log(i))_{\mathrm{pH}} \cdot (\partial \log(i)/\partial \mathrm{pH})_E \quad (2)$$

From the values of 1 and 59 mV of $(\partial \log(i)/\partial \mathrm{pH})_{iE}$ and $(\partial E \partial \mathrm{pH})_i$, respectively, the value of $(\partial E \partial \log(i))_{\mathrm{pH}}$ calculated is 59 mV per decade of current. This value agrees with the Tafel slope obtained. These results are comparable to those of Co-Pi catalyst.[48] Hence, a similar mechanism for oxygen evolution is expected.

The generally accepted mechanism of OER (reaction 1) in neutral or alkaline electrolytes is[26,49]

$$S + OH^- \leftrightharpoons S{-}OH + e^- \quad (3)$$

$$S{-}OH + OH^- \leftrightharpoons S{-}O + H_2O + e^- \quad (4)$$

$$2S{-}O \leftrightharpoons 2S + O_2 \quad (5)$$

where S stands for active sites on the catalyst and S−OH and S−O are the adsorbed intermediates. Detailed analysis of kinetic equations under different conditions are reported by Bockris.[50] Accordingly, 120 mV $decade^{-1}$ is expected for the Tafel slope, if step 3 is the rate-determining step (rds).

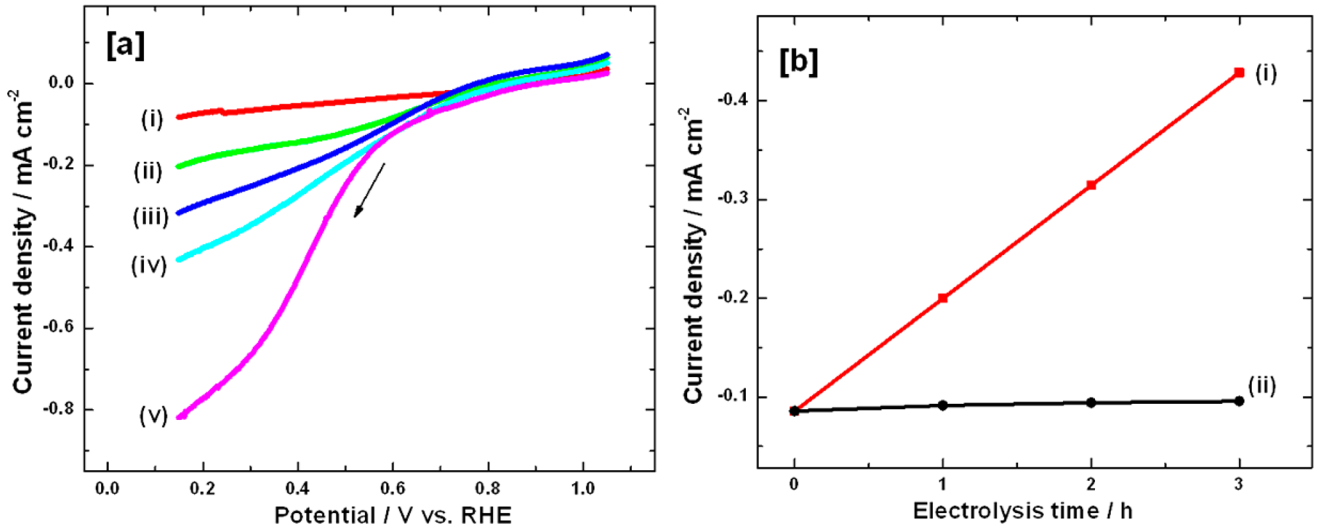

Figure 10. (a) Linear sweep voltammetry for ORR on a Pt RDE in 0.1 M phosphate solution (pH 7.0) under (i) Ar-saturated condition and after oxygen evolution reaction on a Ir-Pi/C electrode at 1.75 V for (ii) 1, (iii) 2, and (iv) 3 h and (v) after purging with O_2 from a cylinder. Scan rate: 10 mV s^{-1} and rotation speed: 2500 rpm. (b) Variation in the ORR current at 0.15 V versus electrolysis time for (i) Ir-Pi/C and (ii) bare carbon.

DOI: 10.1021/acsami.5b02601
ACS Appl. Mater. Interfaces 2015, 7, 15765−15776

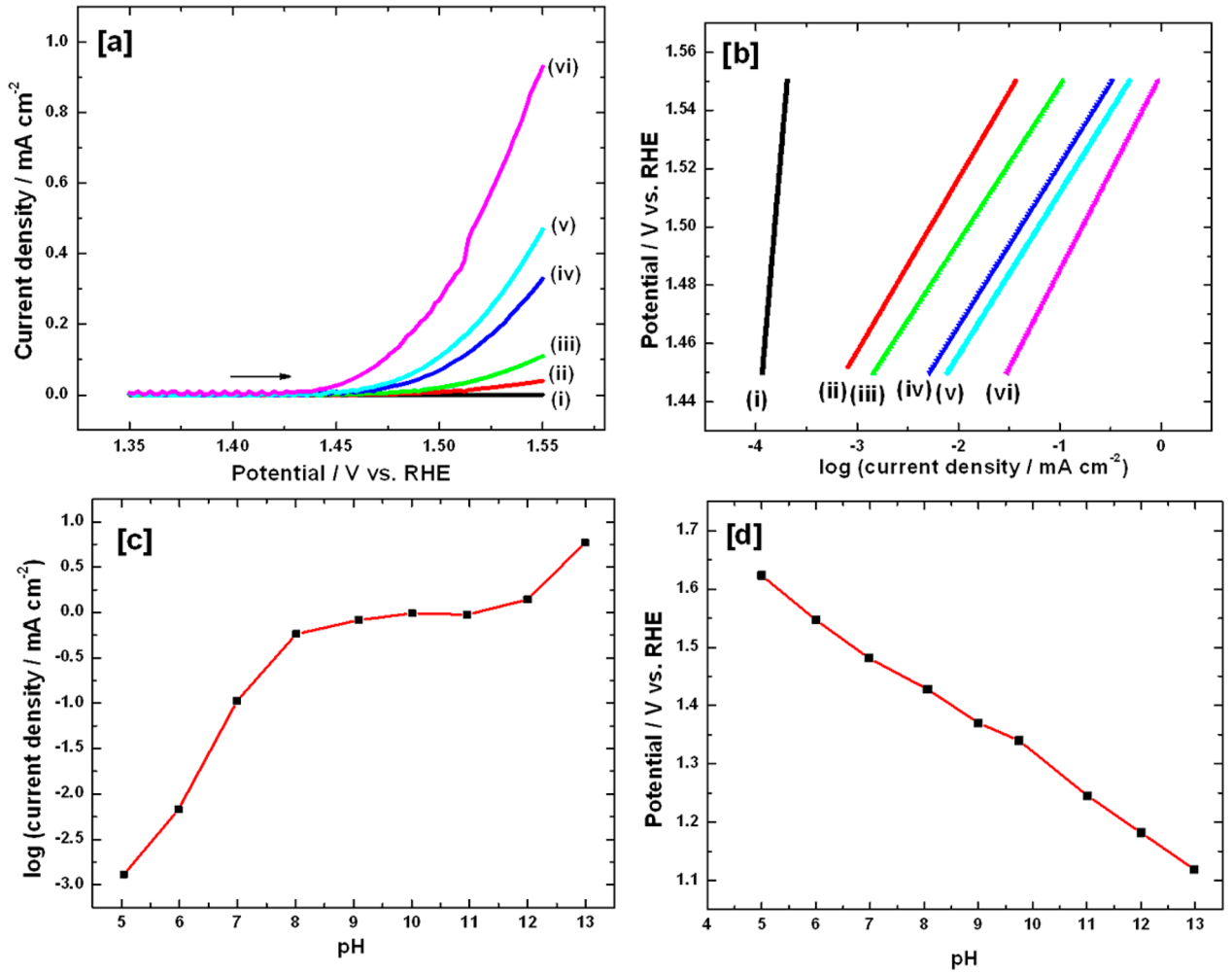

Figure 11. (a) Linear sweep voltammograms of Ir-Pi catalyst prepared using (i) bare carbon paper, (ii) 50, (iii) 100, (iv) 200, (v) 500, and (vi) 1000 mC cm^{-2} in neutral phosphate solution. Scan rate: 0.05 mV s^{-1}. (b) Corresponding Tafel plots, (c) pH dependence of steady state current density at 1.50 V, and (d) pH dependence of steady state electrode potential at 100 μA cm^{-2}. Data in panels c and d are measured at Ir-Pi catalyst prepared using 500 mC cm^{-2} charge.

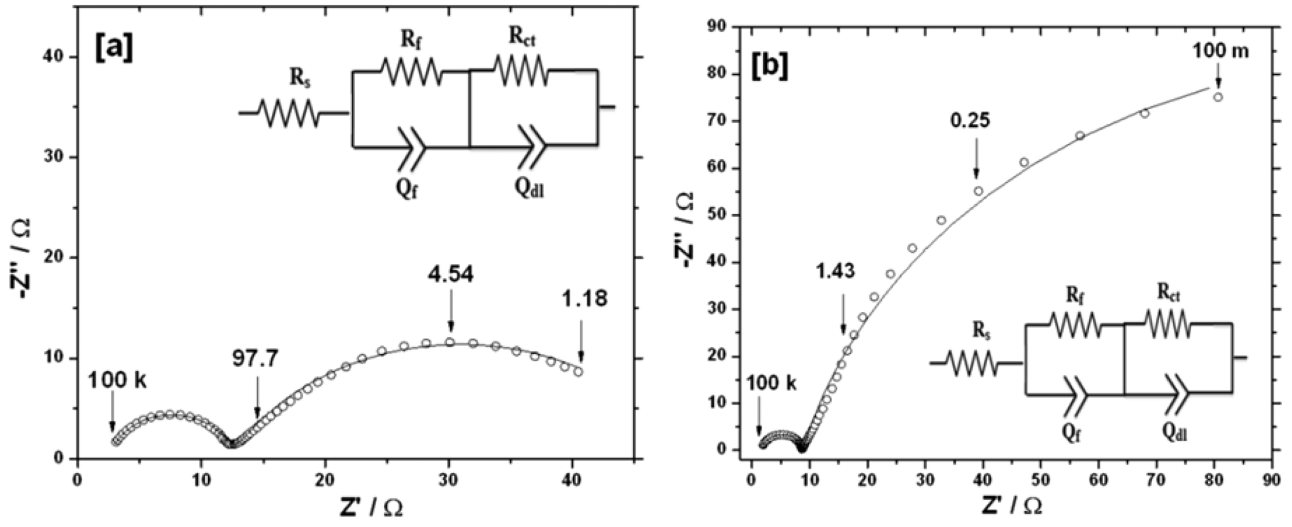

Figure 12. Nyquist plots of (a) Ir-Pi and (b) Co-Pi catalyst coated carbon paper electrodes in 0.1 M neutral phosphate solution at 1.65 V.

Similarly, 40 and 15 mV $decade^{-1}$ are expected for steps 4 and 5, respectively, as the rds. The composition of the catalyst and the reaction conditions are expected to decide which of the three steps or any other step is the rds. As the Tafel slope obtained for OER on Ir-Pi catalyst is 60 mV $decade^{-1}$, the rds appears to be different from steps 3−5. Hu etal.,[51] invoked a

DOI: 10.1021/acsami.5b02601
ACS Appl. Mater. Interfaces 2015, 7, 15765−15776

modification of the above mechanism by an introducing adsorbed intermediate with different energy states, in acidic media. Similarly, in alkaline media also, it is proposed that step 3 can be divided into the following steps:

$$S + OH^- \leftrightharpoons S—OH^* + e^- \quad (6)$$

$$S—OH^* \rightarrow S—OH \quad (7)$$

The adsorbed intermediates S−OH* and S−OH have the same chemical structure, but they differ in their energy states.[51,52] The intermediate S−OH* with higher energy reorganizes to form the lower energy S−OH intermediate. According to the kinetic equations derived by Hu et al.,[51] for the mechanism involving steps 3−7, a Tafel slope of 60 mV decade^{-1} is expected if step 7 is the rds. Thus, the rds of OER on Ir-Pi catalyst is likely to be step 7 with 60 mV decade^{-1} of Tafel slope (Figure 11b).

The catalytic activities of Ir-Pi and Co-Pi are compared from electrochemical impedance spectroscopy (EIS) studies. Both the catalysts were deposited on carbon paper substrate at 1.55 V for 15 min from 0.1 M neutral phosphate solution containing 0.5 mM of the corresponding metal salts. Nyquist plots of Ir-Pi and Co-Pi electrodes in 0.1 M phosphate electrolytes (pH 7.0) at 1.65 V are shown in Figure 12. In both the cases, the complex plane plot shows two broad semicircles. The equivalent circuits corresponding to Ir-Pi and Co-Pi electrodes are also shown in Figure 12 inset. Capacitive elements are replaced by constant phase elements (CPE), denoted by Q and employed for fitting the experimental data. The electrolyte resistance is denoted by R_s. R_f and Q_f denote the resistance and CPE of the catalyst layer whereas R_{ct} and Q_{dl} represent the charge transfer resistance of OER and double layer capacitance. The values of parameters obtained by fitting the impedance data are provided in Table 1. The value of R_{ct} obtained for Ir-Pi

Table 1. Impedance parameters

(A) Ir-Pi catalyst (χ^2 of the fit = 2.8×10^{-4})		
parameters	value	error (%)
R_s (Ω)	2.5	1.9
$Q_f - Y_o$ ($F\ s^{n-1}$)	3.1×10^{-6}	9.4
$Q_f - n$	0.91	0.9
R_f (Ω)	9.8	1.0
$Q_{dl} - Y_o$ ($F\ s^{n-1}$)	0.003	4.0
$Q_{dl} - n$	0.70	1.3
R_{ct} (Ω)	**37.2**	**2.0**
(B) Co-Pi catalyst (χ^2 of the fit = 7.7×10^{-4})		
parameters	value	error (%)
R_s (Ω)	1.7	3.2
$Q_f - Y_o$ ($F\ s^{n-1}$)	2.4×10^{-6}	13.9
$Q_f - n$	0.96	1.3
R_f (Ω)	7.1	1.1
$Q_{dl} - Y_o$ ($F\ s^{n-1}$)	0.009	1.0
$Q_{dl} - n$	0.85	0.6
R_{ct} (Ω)	**201.5**	**1.7**

electrode (37.2 Ω) is smaller by 5.4 times than the value obtained for Co-Pi electrode (201.5 Ω). This indicates a high electrocatalytic OER activity of the Ir-Pi over the Co-Pi catalyst. These results are in agreement with the voltammetric studies.

The stability of the catalyst under water electrolysis is a very important factor for practical application and hence, stability measurements were performed for the Ir-Pi catalyst. For this study, Ir-Pi catalyst was deposited at 1.55 V for 2 h from 0.1 M phosphate buffer (pH 7.0) solution containing 0.5 mM $IrCl_3$. The electrode was rinsed with water and dried overnight at 50 °C. The stability of the electrode was examined by galvanostatic polarization at 1 mA cm^{-2} for 48 h. It is observed that the potential to maintain this current density is almost constant throughout the electrolysis (Figure 13). A slight increase in the

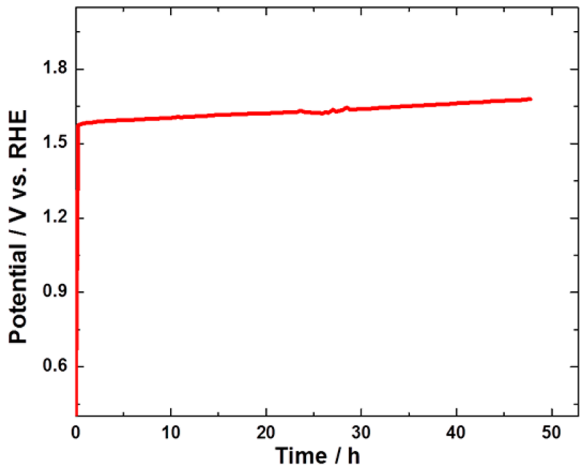

Figure 13. Stability analysis of the Ir-Pi/C electrode by galvanostatic measurement at 1 mA cm^{-2} for 48 h in 0.1 M neutral phosphate buffer solution. Ir-Pi was deposited on carbon paper at 1.55 V for 2 h from 0.1 M neutral phosphate buffer solution containing 0.5 mM $IrCl_3$.

overpotential with time (~100 mV) is attributed to bubble formation on the electrode surface under vigorous oxygen evolution condition. Additionally, no drastic change in the morphology of the catalyst was observed after extended electrolysis (SI, Figure S4), indicating a high structural and functional stability.

4. CONCLUSIONS

An extremely active amorphous water oxidation catalyst namely, Ir-Pi was electrochemically deposited from a neutral phosphate buffer solution containing Ir^{3+} ions. The resultant film on carbon paper electrode exhibited high activity for the electrochemical oxidation of water to O_2 at an overpotential as low as 220 mV in phosphate buffer (pH 7.0) solution. The catalyst exhibited much superior activity in comparison with the well-known IrO_2 and Co-Pi catalysts both in terms of onset potential and current density at any potential in the OER region. Ir-Pi is a promising catalyst for electrochemical splitting of water owing to its easy formation, high activity and stability.

■ ASSOCIATED CONTENT

Supporting Information

Cyclic voltammograms of the Ir-Pi electrodes before and after heat treatment (Figure S1), ECSA measurement (Figure S2), OER activity of the catalysts on FTO substrate (Figure S3), and SEM images after stability test (Figure S4). The Supporting Information is available free of charge on the ACS Publications website at DOI: 10.1021/acsami.5b02601.

■ AUTHOR INFORMATION

Corresponding Author

*E-mail: muni@ipc.iisc.ernet.in. Tel: +91-80-2293 3183.

DOI: 10.1021/acsami.5b02601
ACS Appl. Mater. Interfaces 2015, 7, 15765−15776

Notes

The authors declare no competing financial interest.

REFERENCES

(1) Muradov, N. Z.; Veziroglu, T. N. Green Path From Fossil-based to Hydrogen Economy: An Overview of Carbon-Neutral Technologies. *Int. J. Hydrogen Energy* **2008**, *33*, 6804−6839.

(2) Zutel, A.; Borgschulte, A.; Schlapbach, L. *Hydrogen as a Future Energy Carrier*; Wiley-VCH: Weinheim, Germany, 2008.

(3) Navarro, R. M.; Pena, M. A.; Fierro, J. L. G. Hydrogen Production Reactions from Carbon Feedstocks: Fossil Fuels and Biomass. *Chem. Rev.* **2007**, *107*, 3952−3991.

(4) Pena, M. A.; Gomez, J. P.; Fierro, J. L. G. New catalytic Routes for Syngas and Hydrogen Production. *Appl. Catal., A* **1996**, *144*, 7−57.

(5) van de Krol, R. V.; Liang, Y.; Schoonman, J. Solar Hydrogen Production with Nanostructured Metal Oxides. *J. Mater. Chem.* **2008**, *18*, 2311−2320.

(6) Walter, M. G.; Warren, E. L.; McKone, J. R.; Boettcher, S. W.; Mi, Q.; Santori, E. A.; Lewis, N. S. Solar Water Splitting Cells. *Chem. Rev.* **2010**, *110*, 6446−6473.

(7) Gratzel, M. Photoelectrochemical Cells. *Nature* **2001**, *414*, 338−344.

(8) Cao, R.; Lai, W.; Du, P. Catalytic Water Oxidation at Single Metal Sites. *Energy Environ. Sci.* **2012**, *5*, 8134−8157.

(9) Park, S.; Shao, Y.; Liu, J.; Wang, Y. Oxygen Electrocatalysts for Water Electrolyzers and Reversible Fuel cells: Status and Perspective. *Energy Environ. Sci.* **2012**, *5*, 9331−9344.

(10) Fabbri, E.; Habereder, A.; Waltar, K.; Kotz, R.; Schmidt, T. J. Developments and Perspectives of Oxide Based Catalysts for the Oxygen Evolution Reaction. *Catal. Sci. Technol.* **2014**, *4*, 3800−3821.

(11) Man, I. C.; Su, H. Y.; Calle-Vallejo, F.; Hansen, H. A.; Martinez, J. I.; Inoglu, N. G.; Kitchin, J.; Jaramillo, T. F.; Norskov, J. K.; Rossmeisl, J. Universality in Oxygen Evolution Electrocatalysis on Oxide Surfaces. *ChemCatChem* **2011**, *3*, 1159−1165.

(12) Miles, M. H.; Thomason, M. A. Periodic Variations of Overvoltages for Water Electrolysis in Acid Solutions from Cyclic Voltammetric Studies. *J. Electrochem. Soc.* **1976**, *123*, 1459−1461.

(13) Galizzioli, D.; Tantardhini, F.; Trasatti, S. Ruthenium dioxide: a New Electrode Material. 1. Behaviour in Acid Solutions of Inert Electrolyte. *J. Appl. Electrochem.* **1974**, *4*, 57−67.

(14) Hackwood, S.; Schiavone, L. M.; Dautremont-Smith, W. C.; Beni, G. Anodic Evolution of Oxygen on Sputtered Iridium Oxide Films. *J. Electrochem. Soc.* **1981**, *128*, 2569−2573.

(15) Rogers, D. B.; Shannon, R. D.; Sleight, A. W.; Gillson, J. L. Crystal chemistry of Metal dioxides with Rutile-related Structures. *Inorg. Chem.* **1969**, *8*, 841−849.

(16) Wang, G.; Tsai, D. S.; Huang, Y. S.; Korotcov, A.; Yeh, W. C.; Susanti, D. Selective Growth of IrO_2 Nanorods using Metal-organic Chemical Vapor Deposition. *J. Mater. Chem.* **2006**, *16*, 780−786.

(17) Chen, C. A.; Chen, Y. M.; Huang, Y. S.; Tsai, D. S.; Tiong, K. K.; Du, C. H. Growth and Characterization of V-shaped IrO_2 Nanowedges via Metal-organic Vapor Deposition. *Nanotechnology* **2008**, *19*, 465607−465613.

(18) Ouattara, L.; Fierro, S.; Frey, O.; Koudelka, M.; Comninellis, C. Electrochemical Comparison of IrO_2 prepared by Anodic Oxidation of Pure Iridium and IrO_2 Prepared by Thermal Decomposition of H_2IrCl_6 Precursor Solution. *J. Appl. Electrochem.* **2009**, *39*, 1361−1367.

(19) Arikawa, T.; Takasu, Y.; Murakami, Y.; Asakura, K.; Iwasawa, Y. Characterization of the Structure of RuO_2−IrO_2/Ti Electrodes by EXAFS. *J. Phys. Chem. B* **1998**, *102*, 3736−3741.

(20) Kakooei, S.; Ismail, M. C.; Wahjoed, B. A. Electrochemical Study of Iridium Oxide Coating on Stainless Steel Substrate. *Int. J. Electrochem. Sci.* **2013**, *8*, 3290−3301.

(21) Jung, Y.; Lee, J.; Tak, Y. Electrochromic Mechanism of IrO_2 Prepared by Pulsed Anodic Electrodeposition. *Electrochem. Solid-State Lett.* **2004**, *7*, H5−H8.

(22) Reier, T.; Weidinger, I.; Hildebrandt, P.; Kraehnert, R.; Strasser, P. Electrocatalytic Oxygen Evolution Reaction on Iridium Oxide Model Film Catalysts: Influence of Oxide Type and Catalyst Substrate Interactions. *ECS Trans.* **2013**, *58*, 39−51.

(23) Blakemore, J. D.; Schley, N. D.; Kushner-Lenhoff, M. N.; Winter, A. M.; D'Souza, F.; Crabtree, R. H.; Brudvig, G. W. Comparison of Amorphous Iridium Water-Oxidation Electrocatalysts Prepared from Soluble Precursors. *Inorg. Chem.* **2012**, *51*, 7749−7763.

(24) Indra, A.; Menezes, P. W.; Sahraie, N. R.; Bergmann, A.; Das, C.; Tallarida, M.; Schmeiber, D.; Strasser, P.; Driess, M. Unification of Catalytic Water Oxidation and Oxygen Reduction Reactions: Amorphous Beat Crystalline Cobalt Iron Oxides. *J. Am. Chem. Soc.* **2014**, *136*, 17530−17536.

(25) Tsuji, E.; Imanishi, A.; Fukui, K.-I.; Nakato, Y. Electrocatalytic Activity of Amorphous RuO2 Electrode for Oxygen Evolution in An Aqueous Solution. *Electrochim. Acta* **2011**, *56*, 2009−2016.

(26) Jia, H.; Stark, J.; Zhou, L. Q.; Ling, C.; Sekito, T.; Markin, Z. Different Catalytic Behaviour of Amorphous and Crystalline Cobalt Tungstate for Electrochemical Water Oxiation. *RSC Adv.* **2012**, *2*, 10874−10881.

(27) Esswein, A. J.; Surendranath, Y.; Reecea, S. Y.; Nocera, D. G. Highly Active Cobalt Phosphate and Borate based Oxygen Evolving Catalysts Operating in Neutral and Natural Waters. *Energy Environ. Sci.* **2011**, *4*, 499−504.

(28) Subbaraman, R.; Tripkovic, D.; Chang, K. C.; Strmcnik, D.; Paulikas, A. P.; Hirunsit, P.; Chan, M.; Greeley, J.; Stamenkovic, V.; Markovic, N. M. Trends in Activity for the Water Electrolyser Reactions on 3d M (Ni, Co, Fe, Mn) Hydro(oxy) oxide Cataysts. *Nat. Mater.* **2012**, *11*, 550−557.

(29) Kanan, M. W.; Nocera, D. G. In Situ Formation of an Oxygen-Evolving Catalyst in Neutral Water Containing Phosphate and Co^{2+}. *Science* **2008**, *321*, 1072−1075.

(30) Irshad, A.; Munichandraiah, N. An Oxygen Evolution Co−Ac catalyst − the Synergistic Effect of Phosphate Ions. *Phys. Chem. Chem. Phys.* **2014**, *16*, 5412−5422.

(31) Zaharieva, I.; Cherenev, P.; Risch, M.; Klingan, K.; Kohlhoff, M.; Fischer, A.; Dau, H. Electrosynthesis, Functional, and Structural Characterization of a Water-oxidizing Manganese Oxide. *Energy Environ. Sci.* **2012**, *5*, 7081−7089.

(32) Huynh, M.; Bediako, D. K.; Nocera, D. G. A Functionally Stable Manganese Oxide Oxygen Evolution Catalyst in Acid. *J. Am. Chem. Soc.* **2014**, *136*, 6002−6010.

(33) Wu, Y.; Chen, M.; Han, Y.; Luo, H.; Su, X.; Zang, M.; Lin, X.; Sun, J.; Wang, L.; Deng, L.; Zhang, W.; Cao, R. Fast and Simple Preparation of Iron-Based Thin Films as Highly Efficient Water-Oxidation Catalyst in Neutral Aqueous Solution. *Angew. Chem., Int. Ed.* **2015**, *54*, 4870−4875.

(34) Dinca, M.; Surendranath, Y.; Nocera, D. G. Nickel-borate Oxygen-evolving Catalyst that Functions under Benign Conditions. *Proc. Natl. Acad. Sci. U. S. A.* **2010**, *107*, 10337−10341.

(35) MacDougall, B.; Mitchell, D. F.; Graham, M. J. Galvanostatic Oxidation of Nickel in Borate Buffer Solution. *J. Electrochem. Soc.* **1980**, *127*, 1248−1252.

(36) Yu, F.; Li, F.; Zhang, B.; Li, H.; Sun, L. Efficient Electrocatalytic Water Oxidation by a Copper Oxide Thin Film in Borate Buffer. *ACS Catal.* **2015**, *5*, 627−630.

(37) Kanan, M. W.; Yano, J.; Surendranath, Y.; Dinca, M.; Yachandra, V. K.; Nocera, D. G. Structure and Valency of a Cobalt−Phosphate Water Oxidation Catalyst Determined by in Situ X-ray Spectroscopy. *J. Am. Chem. Soc.* **2010**, *132*, 13692−13701.

(38) Bediako, D. K.; Kaiser, B. L.; Surendranath, Y.; Yano, J.; Yachandra, V. K.; Nocera, D. G. D. G. Nocera Structure−Activity Correlations in a Nickel−Borate Oxygen Evolution Catalyst. *J. Am. Chem. Soc.* **2012**, *134*, 6801−6809.

(39) Lutterman, D. A.; Surendranath, Y.; Nocera, D. G. A Self-Healing Oxygen-Evolving Catalyst. *J. Am. Chem. Soc.* **2009**, *131*, 3838−3839.

(40) Irshad, A.; Munichandraiah, N. EQCM Investigation of Electrochemical Deposition and Stability of Co−Pi Oxygen Evolution Catalyst of Solar Energy Storage. *J. Phys. Chem. C* **2013**, *117*, 8001−8008.

DOI: 10.1021/acsami.5b02601
ACS Appl. Mater. Interfaces 2015, 7, 15765−15776

(41) Terashima, C.; Rao, T. N.; Sarada, B. V.; Spataru, N.; Fujishima, A. Electrodeposition of Hydrous Iridium Oxide on Conductive Diamond Electrodes for Catalytic Sensor Applications. *J. Electroanal. Chem.* **2003**, *544*, 65−74.
(42) Silva, T. M.; Simoes, A. M. P.; Ferreira, M. G. S.; Walls, M.; Cunha Bulo, M. D. Electronic Structure of Iridum Oxide Films Formed in Neutral Phosphate Buffer Solution. *J. Electroanal. Chem.* **1998**, *441*, 5−12.
(43) Korotcov, A.; Huang, Y. S.; Tsai, D. S.; Tiong, K. K. Growth and Characterization of Well Aligned Densely Packed IrO_2 Nanocrystals on Sapphire via Reactive Sputtering. *J. Phys.: Condens. Matter* **2006**, *18*, 1121−1136.
(44) Liu, Y.; Masumoto, H.; Goto, T. Preparation of IrO_2 Thin Films by Oxidating Laser-ablated Ir. *Mater. Trans.* **2004**, *45*, 900−903.
(45) Cobo, S.; Heidkamp, J.; Jacques, P. A.; Fize, J.; Fourmond, V.; Guetaz, L.; Jousselme, B.; Ivanova, V.; Dau, H.; Palacin, S.; Fontecave, M.; Artero, V. A Janus Cobalt-Based Catalytic Material for Electro-Splitting of Water. *Nat. Mater.* **2012**, *11*, 802−807.
(46) Chen, R.; Huang, Y.; Liang, Y.; Tsai, D.; Chi, Y.; Kai, J. Growth Control and Characterization of Vertically Aligned IrO_2 Nanorods. *J. Mater. Chem.* **2003**, *13*, 2525−2529.
(47) Kuch, W.; Schulze, M.; Schnurnberger, W.; Bolwin, K. XPS Line Shape Analysis of Potassium Coadsorbed with Water on Ni(111). *Surf. Sci.* **1993**, *287*−*288*, 600−604.
(48) Surendranath, Y.; Kannan, M. W.; Nocera, D. G. Mechanistic Studies of the Oxygen Evolution Reaction by a Cobalt-Phosphate Catalyst at Neutral P^H. *J. Am. Chem. Soc.* **2010**, *132*, 16501−16509.
(49) Rasiyah, P.; Tseung, A. C. C. A Mechanistic Study of Oxygen Evolution on $NiCo_2O_4$. *J. Electrochem. Soc.* **1983**, *130*, 2384−2386.
(50) Bockris, J. O'M. Kinetics of Activation Controlled Consecutive Electrochemical Reactions: Anodic Evolution of Oxygen. *J. Chem. Phys.* **1956**, *24*, 817−827.
(51) Hu, J.; Zang, J.; Cao, C. Oxygen Evolution Reaction on IrO_2-based DSA Type Electrodes: Kinetics Analysis of Tafel Lines and EIS. *Int. J. Hydrogen Energy* **2004**, *29*, 791−797.
(52) De Faria, L. A.; Boodts, J. F. C.; Trasatti, S. Electrocatalytic Properties of Ternary Oxide Mixtures of Composition $Ru_{0.3}Ti_{(0.7-x)}Ce_xO_2$: Oxygen Evolution from Acidic Solution. *J. Appl. Electrochem.* **1996**, *26*, 1195−1199.

DOI: 10.1021/acsami.5b02601
ACS Appl. Mater. Interfaces 2015, 7, 15765−15776